

## Periodic-cluster calculations of the valence states and native defects in diamond, silicon, germanium, ZnS, ZnSe, and SiC

Wanda V. M. Machado and Jorge A. Kintop

*Instituto de Física, Universidade de São Paulo, Caixa Postal 20516, 01498 São Paulo, Brazil*

Manoel L. De Siqueira\* and Luiz G. Ferreira

*Instituto de Física, Universidade Estadual de Campinas, Caixa Postal 6165, 13081 Campinas, Brazil*

(Received 16 September 1992; revised manuscript received 1 December 1992)

We present the results of band calculations and of native defects on diamond, Si, Ge, ZnS, ZnSe, and SiC by means of periodic clusters. We study the convergence of the results with cluster size. For clusters as small as eight atoms, eigenvalues and eigenfunctions seem to be converged. Compared to nonperiodic clusters, the present technique has the advantage of establishing a one-to-one correspondence to the eigenvalues of a full band calculation (infinite-sized cluster). Compared to the full band calculation, the periodic-cluster technique is equivalent to a calculation with "special points" integration in the Brillouin zone. The periodic-cluster calculation is useful when a spectrum "discretization" is desired, for instance, in the calculation of defects. We illustrate this point by presenting the results of calculations on native defects in these semiconductors. Our results for the valence states are in excellent agreement with experiment. In other instances, our results are able to give a theoretical interpretation to experiment.

### I. INTRODUCTION

Periodic clusters are infinite crystals for which one imposes the periodic boundary conditions after a small number of cells. They are a convenient description of the crystal when it is advantageous to have a discrete set of eigenvalues instead of the continuum of the truly infinite crystal.<sup>1-5</sup> The discretization of the spectrum, when it does not hide any important physical effect, is able to simplify enormously the solution of some quantum-mechanical problems, for instance, in the calculation of the defect levels.<sup>6,7</sup> Though the periodic clusters have some remarkable advantages with respect to nonperiodic clusters,<sup>8-10</sup> because of their symmetry properties (Sec. II), only exceptionally have they been used in the calculation of the one-electron eigenvalues.<sup>3</sup>

To fix our notation, we present in Table I the first four cubic periodic clusters of the diamond (and zinc-blende) lattice. In each case we give the number of atoms included, the unit vectors of the cluster, which is the repeating unit, the atomic positions, and the size of the symmetry group. The symmetry group of a periodic cluster is a finite space group (FSG), which is a subgroup of the crystal infinite space group (ISG). This latter property makes the periodic cluster more convenient than nonperiodic clusters. Further, the eigenvalues in a periodic-cluster calculation may be simply identified to those of the full band-structure calculation, an identification that is impossible in the nonperiodic-cluster calculations.

The calculation of one-electron levels with periodic clusters becomes equivalent to a band-structure calculation with "special points"<sup>11-15</sup> if the special points of the band calculation are chosen to be those that generate the representations of the FSG (Table I), and their weights coincide with the relative occupation numbers in the periodic-cluster calculation. This coincidence happens, at

least for the clusters with 2, 8, 16, and 32 atoms, if one uses the Chadi and Cohen rule<sup>12</sup> to generate weights for the special points of Table I. Thus, in this case, the two procedures, namely the special-points band calculation and the periodic-cluster calculation, become equivalent and necessarily lead to the same results. The difference between the two calculations is only conceptual. It must be mentioned that usually the special points are chosen to form a minimal grid in  $k$  space displaced<sup>14</sup> from the origin ( $\Gamma$ ), while the periodic-cluster technique leaves no room for such displacements. For instance, comparing the four sets of special points in Table I with the first four sets of Moreno and Soler,<sup>15</sup> one notices that instead of the set corresponding to eight atoms, with points  $\Gamma$  and  $X$ , those authors would recommend just point  $L$ . Choosing the special points is usually made by zeroing the first few terms of a Fourier expansion with a minimal set of points, while in the present technique one starts in the real space by choosing the periodic cluster.

Then one could ask why bother with periodic clusters when the more conventional special-points band calculation is able to give the same results. First, we think that the necessary study of the size effect,<sup>4</sup> which is the convergence of the results with the size of the periodic cluster, is in itself very enlightening. Second, from a periodic-cluster calculation of the discrete spectrum one could, in principle, restore the band continuum by means of the  $k \cdot p$  perturbation,<sup>16</sup> so that there would be no loss of information in these calculations, though  $k \cdot p$  might not be very practical. Third, the periodic-cluster calculation seems to be the most reliable means to perform the useful discretization of the band continuum. Fourth, the calculation of defect levels by means of periodic clusters is a simple extension of the pure crystal calculation, uses the same basis, and keeps close relation to the *large unit cell* method.<sup>17</sup>

TABLE I. Cubic periodic clusters of the diamond (and zinc-blende) structure and their special points equivalents in a full band calculation. The lattice parameter  $a = 4$ .

No. of atoms	Unit vectors	Atomic positions	Group dimens.	Full band equivalent special points	weights
2	(022)	000,111	48(24)	$\Gamma$	1
	(202)				
	(220)				
8	(400)	000,022,202,220 111,133,313,331	192(96)	$\Gamma$	$\frac{1}{4}$
	(040)			$X$	$\frac{3}{4}$
	(004)				
16	(044)	000,022,202,220 400,422,242,224 111,133,313,331 511,533,353,335	384(192)	$\Gamma$	$\frac{1}{8}$
	(404)			$X$	$\frac{3}{8}$
	(440)			$L$	$\frac{4}{8}$
32	(-444)	000,022,202,220 400,422,242,224 040,004,620,206	768(384)	$\Gamma$	$\frac{1}{16}$
	(4-44)	062,602,260,026		$X$	$\frac{3}{16}$
	(44-4)	111,133,313,331		$\Sigma \frac{\pi}{a}(011)$	$\frac{12}{16}$
		511,533,353,335			
		151,115,731,317 173,713,371,137			

In this paper we present results of periodic-cluster calculations on semiconductors with the diamond and zinc-blende structures, pure and with native defects, *at the experimental lattice constant of the pure semiconductor*. Among the native defects that we calculated, mostly interstitials and vacancies, we cannot fail to mention the defect created by the electronic excitation of some valence energy levels.<sup>18-20</sup> A typical case is that of the Zn  $3d$  levels in ZnS and ZnSe. By promoting one of their electrons to the conduction band, one leaves behind not a Bloch state hole, but a hole that is mostly dense at only one of the Zn atoms and that, for this very reason, breaks the translational symmetry of the crystal.

We exclude from our calculations of native defects all lattice distortions, which are important only for vacancies. We are most interested in the valence-band states, and not in the conduction states or in the gap defect states, because there the *local-density approximation* calculations are known to give results comparable to experiment, while the conduction states need quasiparticle corrections. Our calculations are "all-electron" (not pseudopotential based) and nonrelativistic. Among the semiconductors we calculated, the relativistic corrections are only important for those valence states that are based on the  $4s$  Ge and Se orbitals. For the other valence states the relativistic corrections are negligible.

## II. SYMMETRY OF PERIODIC CLUSTERS

In usual group theory, as applied to crystals, it is common practice to limit the group of symmetry operations by forcing the so-called periodic boundary conditions

after a very large number of cells, say  $10^{23}$ . The periodic boundary conditions, instead of other boundary conditions at the surface, have the virtue of being consistent with the symmetry which is the most important in a crystal: the translational symmetry. The resulting set of symmetry operations, containing rotations, inversions, glide planes, screw axes, and translations, forms a group, the space group of the crystal. Normally the periodic boundary conditions are made after so many cells that one rarely needs to recall that the space group is truly a finite group and commonly deals with it as if it were infinite.

The main idea of the periodic-cluster technique is to apply the periodic boundary conditions after a much reduced number of crystal cells. For instance, in Table I we list four different periodic clusters with 2 atoms (1 crystal cell), 8 atoms (4 crystal cells), 16 atoms (8 crystal cells), and 32 atoms (16 crystal cells). In each case, the crystal is thought to repeat itself after a translation which is an integer combination of the unit vectors shown in Table I, instead of only repeating itself after  $10^{23}$  crystal cells. The symmetry group in the present case is also a space group, and due to its smallness we call it the *finite space group* (FSG), in opposition to the space group of the almost infinite crystal which is called the *infinite space group* (ISG). If the infinite crystal is made of an integer number of periodic clusters, one can write the obvious relation between the element of the two space groups:

$$(O_{\text{ISG}}) = (O_{\text{FSG}}) \otimes T, \quad (1)$$

meaning that any operation  $O_{\text{ISG}}$  of the ISG is the prod-

uct of an operation  $O_{\text{FSG}}$  of the FSG times a translation  $T$  made of those cluster unit vectors of Table I.

The equation above gives us a recipe on how to find the irreducible representations of the FSG. Indeed, consider the representations of the infinite space group that are invariant under the translations of the cluster. According to the equation, these representations of the ISG are also representations of the FSG, and if they were irreducible in the ISG they are also irreducible in the FSG. Now, the irreducible representations of the ISG have been discussed by Koster<sup>21</sup> and are based on the many wave-vector points of the Brillouin zone. Accordingly, the irreducible representations of the FSG are based on the representations of the groups of the wave vectors corresponding to periodic functions whose period is the cluster. For the clusters tabulated in Table I, the irreducible representations of FSG are the irreducible representations of the ISG at the special points.

Therefore, finding the irreducible representations of the FSG is not specially difficult because one has the ISG

as a reference. Finding the classes and projection operators is perhaps more difficult, but nevertheless a standard group theoretical work. In Table II we present the character table for the FSG of the 8-atom clusters (diamond and zinc blende), and in Table III the character table for the 16-atom clusters. In both cases the irreducible representations are labeled according to the corresponding Brillouin zone point and to the Slater notation for the corresponding representations of the groups of the wave vectors.<sup>22</sup> These tables are constructed in such a way that the reduction of the diamond FSG into the zinc-blende FSG, and into the point group  $T_d$ , can be readily read from them. Some features of these tables can be promptly understood. For instance, since there are three equivalent points  $X$ , the  $X$  representations have dimensions that are multiples of 3. Analogously, the  $L$  representations in Table III have dimensions a multiple of 4. Other features are more surprising, as the way the many group elements fall into classes. These tables will be useful in understanding the many calculated results.

TABLE II. Character table for the 8-atom diamond ( $O_h^7$ ) and the 8-atom zinc-blende ( $T_d^2$ ) periodic-cluster groups, and for the point group  $T_d$ . The classes are given by the angle of rotation, axis,  $-1$  ( $+1$ ) if the rotation is (is not) followed by inversion, and translation vector. Classes 2 and 4 of the diamond group split into two classes in the zinc-blende group. The lattice parameter  $a=4$ . The representations of the zinc-blende group are in parentheses ( ), and the representations of the point group  $T_d$  between square brackets [ ]. The representations are named according to the representations of the groups of the wave vectors. We also indicate what atomic functions  $s, p, d$  generate each representation.

Class	1	2	3	4	5	6	7	8	9	10	11	12	13	14
Angle	0	$\pi$	$\frac{2\pi}{3}$	$\frac{\pi}{2}$	$\pi$	0	$\pi$	$\pi$	0	$\pi$	$\frac{2\pi}{3}$	$\frac{\pi}{2}$	$\pi$	$\pi$
Axis	1	1	1	1	1	1	1	1	1	1	1	1	1	1
	0	0	1	0	1	0	0	1	0	0	1	0	1	1
	0	0	1	0	0	0	0	0	0	0	1	0	0	0
Inversion	1	1	1	-1	-1	1	1	-1	-1	-1	-1	1	1	1
Translation	0	0 0	0	0 2	0	2	2	2	1	1	1	1	-1	1
	0	0 2	0	0 0	0	0	2	0	1	1	1	1	1	1
	0	0 2	0	0 2	0	2	0	2	1	1	1	1	-1	1
Elements ( $O_h^7$ )	1	6	32	24	12	3	6	12	4	12	32	24	12	12
( $T_d^2$ )	1	3 3	32	12 12	12	3	6	12						
( $T_d$ )	1	3	8	6	6									
$\Gamma_1(\Gamma_1)[a_1]s$	1	1	1	1	1	1	1	1	1	1	1	1	1	1
$\Gamma_2(\Gamma_2)[a_2]$	1	1	1	-1	-1	1	1	-1	1	1	1	-1	-1	-1
$\Gamma_{12}(\Gamma_{12})[e]d$	2	2	-1	0	0	2	2	0	2	2	-1	0	0	0
$\Gamma'_{15}(\Gamma_{25})[t_1]$	3	-1	0	1	-1	3	-1	-1	3	-1	0	1	-1	-1
$\Gamma'_{25}(\Gamma_{15})[t_2]pd$	3	-1	0	-1	1	3	-1	1	3	-1	0	-1	1	1
$\Gamma'_1(\Gamma_2)[a_2]$	1	1	1	-1	-1	1	1	-1	-1	-1	-1	1	1	1
$\Gamma'_2(\Gamma_1)[a_1]s$	1	1	1	1	1	1	1	1	-1	-1	-1	-1	-1	-1
$\Gamma'_{12}(\Gamma_{12})[e]d$	2	2	-1	0	0	2	2	0	-2	-2	1	0	0	0
$\Gamma_{15}(\Gamma_{15})[t_2]pd$	3	-1	0	-1	1	3	-1	1	-3	1	0	1	-1	-1
$\Gamma_{25}(\Gamma_{25})[t_1]$	3	-1	0	1	-1	3	-1	-1	-3	1	0	-1	1	1
$X_1$	6	2	0	0	2	-2	-2	-2	0	0	0	0	0	0
$=(X_1)[a_1 + e]sd$	3	3 -1	0	1 -1	1	-1	-1	-1						
$+(X_3)[t_2]pd$	3	-1 3	0	-1 1	1	-1	-1	-1						
$X_2$	6	2	0	0	-2	-2	-2	2	0	0	0	0	0	0
$=(X_2)[a_2 + e]d$	3	3 -1	0	-1 1	-1	-1	-1	1						
$+(X_4)[t_1]$	3	-1 3	0	1 -1	-1	-1	-1	1						
$X_3(X_5)[t_1 + t_2]pd$	6	-2	0	0	0	-2	2	0	0	0	0	0	2	-2
$X_4(X_5)[t_1 + t_2]pd$	6	-2	0	0	0	-2	2	0	0	0	0	0	-2	2

The equation above, relating the space groups ISG and FSG, establishes a clear meaning to the “special points” corresponding to the periodic cluster. Indeed, at those points of the Brillouin zone representing Bloch functions that have the period of the cluster, the irreducible representations of the FSG coincide with those of the ISG. The set of such points forms a grid in the  $k$  space with a mesh volume which is the reciprocal of the cluster volume in the real space. Of course, point  $\Gamma$ , the center of the Brillouin zone, always belongs to this set because the Bloch functions there are periodic in the lattice. Compared with the most common “special-points” construction,<sup>14</sup> the set of periodic-cluster special points is not displaced so as to minimize the number of points in the set. While the usual construction is appropriate because

it generates less points in the set, the periodic-cluster construction uses points with higher symmetry (less numerical work per point) and preserves the real-space description, which is most important to us.

### III. METHODS

#### A. The linearized variational cellular method

We now review our total energy local-density approximation (LDA) method because it is not in the mainstream of band calculation techniques such as linearized augmented plane wave (LAPW), linearized muffin-tin orbital (LMTO), and norm-conserving pseudopotentials. Our version of the cellular method has been described in

TABLE III. Character table for the 16-atom diamond ( $O_h^7$ ) and the 16-atom zinc-blende ( $T_d^2$ ) periodic-cluster groups, and for the point group  $T_d$ . The classes are given by the angle of rotation, axis,  $-1$  ( $+1$ ) if the rotation is (is not) followed by inversion, and translation vector. Classes 2 and 4 of the diamond group split into two classes in the zinc-blende group. The lattice parameter  $a=4$ . The representations of the zinc-blende group are in parentheses ( ), and the representations of the point group  $T_d$  between square brackets [ ]. The representations are named according to the representations of the groups of the wave vectors. We also indicate what atomic functions  $s, p, d$  generate each representation.

Class	1	2	3	4	5	6	7	8	9	10	11	12	13	14	15	16	17	18	19	20
Angle	0	$\pi$	$\frac{2\pi}{3}$	$\frac{\pi}{2}$	$\pi$	0	0	$\pi$	$\frac{2\pi}{3}$	$\pi$	$\pi$	0	0	$\pi$	$\frac{2\pi}{3}$	$\frac{2\pi}{3}$	$\frac{\pi}{2}$	$\pi$	$\pi$	$\pi$
Axis	1	1	1	1	1	1	1	1	1	1	1	1	1	1	1	1	1	1	1	1
	0	0	1	0	1	0	0	0	1	1	1	0	0	0	1	1	0	1	1	1
	0	0	1	0	0	0	0	0	1	0	0	0	0	0	1	1	0	0	0	0
Inversion	1	1	1	-1	-1	1	1	1	1	-1	-1	-1	-1	-1	-1	-1	1	1	1	1
Translation	0	0 0	0	0 2	0	2	4 2	2	2	0	4	1	1	1	1	1	1	1	1	-3
	0	0 2	0	0 0	0	2	0 2	2	2	0	0	1	1	1	-1	1	1	1	1	-1
	0	0 2	0	0 2	0	0	0 0	0	2	0	1	-3	1	-1	1	1	1	1	-1	1
Elements ( $O_h^7$ )	1	12	32	48	12	6	1 12	32	24	12	4	4	24	32	32	48	12	24	12	12
( $T_d^2$ )	1	66	32	24 24	12	6	1 12	32	24	12										
( $T_d$ )	1	3	8	6	6															
$\Gamma_1(\Gamma_1)[a_1]s$	1	1	1	1	1	1	1	1	1	1	1	1	1	1	1	1	1	1	1	1
$\Gamma_2(\Gamma_2)[a_2]$	1	1	1	-1	-1	1	1	1	1	-1	-1	1	1	1	1	1	-1	-1	-1	-1
$\Gamma_{12}(\Gamma_{12})[e]d$	2	2	-1	0	0	2	2	2	-1	0	0	2	2	2	-1	-1	0	0	0	0
$\Gamma'_{15}(\Gamma_{25})[t_1]$	3	-1	0	1	-1	3	3	-1	0	-1	-1	3	3	-1	0	0	1	-1	-1	-1
$\Gamma_{25}(\Gamma_{15})[t_2]pd$	3	-1	0	-1	1	3	3	-1	0	1	1	3	3	-1	0	0	-1	1	1	1
$\Gamma'_1(\Gamma_2)[a_2]$	1	1	1	-1	-1	1	1	1	1	-1	-1	-1	-1	-1	-1	-1	1	1	1	1
$\Gamma'_2(\Gamma_1)[a_1]s$	1	1	1	1	1	1	1	1	1	1	1	-1	-1	-1	-1	-1	-1	-1	-1	-1
$\Gamma'_{12}(\Gamma_{12})[e]d$	2	2	-1	0	0	2	2	2	-1	0	0	-2	-2	-2	1	1	0	0	0	0
$\Gamma_{15}(\Gamma_{15})[t_2]pd$	3	-1	0	-1	1	3	3	-1	0	1	1	-3	-3	1	0	0	1	-1	-1	-1
$\Gamma_{25}(\Gamma_{25})[t_1]$	3	-1	0	1	-1	3	3	-1	0	-1	-1	-3	-3	1	0	0	-1	1	1	1
$X_1$	6	2	0	0	2	-2	6	-2	0	-2	2	0	0	0	0	0	0	0	0	0
$=(X_1)[a_1+e]sd$	3	3	-1	0	1	-1	3	-1	0	-1	1									
$+(X_3)[t_2]pd$	3	-1	3	0	-1	1	3	-1	0	-1	1									
$X_2$	6	2	0	0	-2	-2	6	-2	0	2	-2	0	0	0	0	0	0	0	0	0
$=(X_2)[a_2+e]d$	3	3	-1	0	-1	1	3	-1	0	1	-1									
$+(X_4)[t_1]$	3	-1	3	0	1	-1	3	-1	0	1	-1									
$X_3(X_5)[t_1+t_2]pd$	6	-2	0	0	0	-2	6	2	0	0	0	0	0	0	0	0	0	2	-2	2
$X_4(X_5)[t_1+t_2]pd$	6	-2	0	0	0	-2	6	2	0	0	0	0	0	0	0	0	0	-2	2	-2
$L_1(L_1)[a_1+t_2]spd$	4	0	1	0	2	0	-4	0	-1	0	-2	-2	2	0	-1	1	0	-2	0	2
$L_2(L_2)[a_2+t_1]$	4	0	1	0	-2	0	-4	0	-1	0	2	-2	2	0	-1	1	0	2	0	-2
$L_3(L_3)[e+t_1+t_2]pd$	8	0	-1	0	0	0	-8	0	1	0	0	-4	4	0	1	-1	0	0	0	0
$L'_1(L_2)[a_2+t_1]$	4	0	1	0	-2	0	-4	0	-1	0	2	2	-2	0	1	-1	0	-2	0	2
$L'_2(L_1)[a_1+t_2]spd$	4	0	1	0	2	0	-4	0	-1	0	-2	2	-2	0	1	-1	0	2	0	-2
$L'_3(L_3)[e+t_1+t_2]pd$	8	0	-1	0	0	0	-8	0	1	0	0	4	-4	0	-1	1	0	0	0	0

Ref. 23 and in the references quoted therein. Here we discuss only those features of the method connected with its precision, leaving out the discussion on its speed and mathematical formalism to the reference. The reader must be warned that the term “cellular” is very broad and may refer to many very different methods. Usually the term is applied to those methods based on a space partitioning into polyhedra (and that excludes methods such as LAPW and LMTO, which use spheres) and point matching the wave functions and potentials at the surface of the polyhedra. Even so, there are many versions of cellular methods, from the earliest versions, with non-variational matching, of Slater<sup>24</sup> and Altmann<sup>25</sup> to newer variational versions.<sup>26</sup> On and off, the “cellular” idea keeps appearing in the literature in different contexts.<sup>27</sup>

We use the following total-energy functional:

$$E[\psi, V, n, c] = \sum_i K[\psi_i] + U[n - p, c] - S[p] + E_{xc}[n] + \int d^3r V(\mathbf{r}) \left[ \sum_i \psi_i(\mathbf{r})^* \psi_i(\mathbf{r}) - n(\mathbf{r}) \right], \quad (2)$$

whose terms have the following meaning.

(i)  $K[\ ]$  is the kinetic-energy term of Kohn and Sham. In the cellular method, aside from volume integrals, one also uses surface integrals at the cell boundaries that guarantee a variational matching of the wave functions.<sup>28,29,23</sup>

(ii)  $E_{xc}$  is the LDA exchange-correlation functional. We used the Gunnarsson-Lundqvist expression.<sup>30</sup> Self-consistent runs with the Cepperley-Alder expression as parametrized by Perdew and Zunger<sup>31</sup> produced level shifts of at most 0.02 eV.

(iii)  $U[\ ] - S[\ ]$ . Here  $p$  is the proton number density, that is a collection of  $\delta$  functions (we make an “all-electron” calculation, not pseudopotential). Thus  $S[\ ]$  is the nuclear self-energy that must be subtracted from the electrostatic self-interaction of the electronic  $n$  and nuclear  $p$  charge densities. The functional  $U[\ ]$  of electrostatic energy, instead of being written in the most conventional form

$$U[q] = \int d^3r \int d^3r' \frac{q(\mathbf{r})q(\mathbf{r}')}{|\mathbf{r} - \mathbf{r}'|}, \quad (3)$$

is written as

$$U[q, c] = \int d^3r q(\mathbf{r})c(\mathbf{r}) - \frac{1}{16\pi} \int d^3r \nabla c \cdot \nabla c + (\text{cell surface terms}), \quad (4)$$

where  $c$  is the Coulomb potential satisfying the Poisson equation resulting from

$$\frac{\delta U}{\delta c} = 0. \quad (5)$$

In the cellular method, the last expression for the functional  $U[\ ]$  is more convenient than the conventional expression. As in the case of the kinetic-energy functional, we add surface integrals to make variational the matching of  $c$  at the cell boundaries.

(iv) The last term of the total-energy functional is a

modification of the LDA total energy that allows us to deal with different number densities  $n(\mathbf{r})$  and  $\sum_i \psi_i(\mathbf{r})^* \psi_i(\mathbf{r})$ .  $V(\mathbf{r})$  is a Lagrange multiplier function for the condition

$$\sum_i \psi_i(\mathbf{r})^* \psi_i(\mathbf{r}) - n(\mathbf{r}) = 0, \quad (6)$$

restricting the minimization of the total energy. This term was originally proposed in connection with a study of the muffin-tin potentials in the multiple-scattering method,<sup>32</sup> the latter used to generate empirical atomic potentials,<sup>33</sup> and was incorporated into our work with the cellular method from the earliest days. This term allows modeling the true number density into  $n(\mathbf{r})$ . In that, the term is analogous to the Wendel-Martin procedure,<sup>34</sup> and to the Harris functional.<sup>35</sup>

With the terms above, the total energy becomes stationary (not minimum, even for the ground state) with respect to variations in the one-particle wave functions  $\psi$ , the Coulomb potential  $c$ , the model number density  $n$ , and the Lagrange multiplier  $V$ . Equating to zero the first-order variations of the total energy  $E$  leads to the following results.

(i)  $\delta E / \delta \psi = 0$  leads to the one-electron Kohn-Sham Schrödinger equations whose potential is the Lagrange multiplier function  $V(\mathbf{r})$ . This allows us to call  $V$  the Schrödinger equation potential. In the variational cellular method, because of the surface terms, this equation also leads to the matching of the wave function and its normal derivative at the cell boundaries.

(ii)  $\delta E / \delta c = 0$  leads to the Poisson equation for the Coulomb potential  $c$ , and to the matching of  $c$  and of its normal derivative at the cell boundaries.

(iii) A variation on the model density  $n$  leads to

$$\delta E = \int d^3r \delta n(\mathbf{r}) [c(\mathbf{r}) + \delta E_{xc} / \delta n - V(\mathbf{r})] = 0, \quad (7)$$

which is zero if the Schrödinger equation potential equals the Coulomb plus exchange-correlation potentials.

(iv) A variation on the Schrödinger equation potential  $V$  leads to

$$\delta E = \int d^3r \delta V(\mathbf{r}) \left[ \sum_i \psi_i(\mathbf{r})^* \psi_i(\mathbf{r}) - n(\mathbf{r}) \right] = 0, \quad (8)$$

which is null if the model number density  $n$  coincides with the true number density.

In the cellular method that we used, the wave functions  $\psi$  and Coulomb potential  $c$  were expanded in a spherical harmonics series up to  $l=4$ . For the diamond structure, with atomic and empty cells,  $l=4$  is already over killing the problem so that, for all practical purposes, we may say that the one-electron Schrödinger equations and the Poisson equation were solved exactly. The model number density  $n$  and the Schrödinger equation potential  $V$  were made spherical inside each cell. The well-known success of the Harris functional (for example, see Ref. 36) suggested to us that modeling  $n$  and  $V$  would be only a source of minor errors, a prediction well confirmed by our results.

In all our calculations we used the experimental lattice constants. We filled the space with polyhedral cells centered at the atoms and at the interstitial positions of the

diamond lattice. In the method that we use,<sup>23</sup> the polyhedral cells are further divided by inscribed spheres. The wave functions  $\psi$  and Coulomb potential  $c$  have different expansions inside the inscribed sphere and in the region between the sphere and the polyhedral cell boundaries. Of course the two expansions match at the sphere in the variational solution, a typical feature of the cellular method.

Inside the inscribed spheres, the Schrödinger equation potential  $V(r)$  and the model density  $n(r)$  were taken as the spherical averages, according to Eqs. (7) and (8). In the region between the inscribed sphere and the cell boundary we used two different expansions for  $V(r)$  and  $n(r)$ . The expansion most frequently used had three terms,

$$V(r) = B_1/r + B_2 + B_3 r \quad [\text{and } n(r)] \quad (9)$$

with  $B_1$ ,  $B_2$ , and  $B_3$  chosen so that Eqs. (7) and (8) were satisfied. The second expansion was simpler and had just one term,

$$V(r) = B_2 \quad [\text{and } n(r)], \quad (10)$$

the constant  $B_2$  depending on the cell. In this case the potential and model density become muffin tin in each cell (not muffin tin in the whole crystal). Different ways to define the potential  $V(r)$  and the model density  $n(r)$  at those regions led to slightly different results, with deviations on the order of a few tenths of 1 eV. Of course, results with the three term expansions are to be preferred.

### B. The transition state

In the local-density approximation the excitation energies are calculated according to the following equation:<sup>37</sup>

$$\frac{dE}{dw_i} = \epsilon_i, \quad (11)$$

relating the derivative of the total energy  $E$  with respect to the fractional occupation number  $w_i$  and the one-electron eigenvalue  $\epsilon_i$ . In most cases, the eigenvalues are linear with the occupation, so the derivative

$$\frac{d\epsilon_i}{dw_i} = 2S_i \quad (12)$$

is independent of the level occupation. Then excitation energy becomes the difference between half occupied energy levels (transition state) which differ from the ground-state energy levels according to

$$\epsilon_i(\frac{1}{2}) - \epsilon_i(0) = S_i. \quad (13)$$

Moreover  $S_i$  could be calculated by first-order perturbation theory to give

$$S_i = \int d^3r \int d^3r' \frac{n_i(\mathbf{r})n_i(\mathbf{r}')}{|\mathbf{r}-\mathbf{r}'|} + \frac{1}{2} \int d^3r \int d^3r' n_i(\mathbf{r}') \frac{\delta^2 E_{xc}}{\delta n(\mathbf{r})\delta n(\mathbf{r}')} n_i(\mathbf{r}). \quad (14)$$

The first term on the right-hand side of the above equation gives meaning to the difference between the half-

occupied level and the ground-state level. It is obviously the self-interaction electrostatic energy and it is always positive or zero. The second term, which is negative, is an exchange-correlation correction to that self-interaction. This correction is usually dominated by the electrostatic self-interaction. The self-interaction correction above, due to its dependence on  $n^2$ , is zero if one is dealing with a Bloch state that spreads in the whole crystal. For most of our cluster states, though not exactly null, the self-interaction is still negligible. The self-interaction is only important when dealing with wave functions that concentrate at a defect. In those cases we calculate it as the difference between the transition state energy and the energy level at the ground state.

The term self-interaction is mostly used in connection with the SIC method of Perdew and Zunger.<sup>31</sup> Their expression and ours have some similarity but are not identical. Our expression is always calculated by the transition state. The reader is warned not to confuse the transition state self-interaction that we use with the SIC method.

## IV. RESULTS AND DISCUSSION

### A. Perfect Si and Ge

In Tables IV and V we present the eigenvalues of Si and Ge, for the 2-, 8-, and 16-atom periodic clusters, together with the full band results of Hybertsen and Louie.<sup>38</sup> The full band results should be understood as equivalent to an infinite-sized periodic cluster, and compared to our results, which have a residual potential shape approximation [Eq. (9)]. A stronger potential shaping is made when we use Eq. (10) instead of Eq. (9), that is, when the potential becomes muffin tin per cell. In the case of Si, for the 8-atom cluster, we also present the calculated results within the latter approximation. One sees that potential shaping is no problem when one uses the dense packing of atomic and empty cells as we did.

Most remarkable in Tables IV and V is the fast convergence of our results with the size of the periodic cluster. The self-consistent potentials for the 2-atom clusters are already very good starting points for the self-consistent iterations for larger clusters. Not only the eigenvalues seem to have converged in the 8-atom cluster, but the eigenfunctions too; otherwise, out of the wrong momentum matrix elements at  $\Gamma$  one would never obtain the eigenvalues at  $X$ , for instance, by  $k \cdot p$  perturbation. The simultaneous convergence of the eigenvalues at  $\Gamma$  and  $X$  gives an assurance that the eigenfunctions have also converged.

In another respect, the convergence is also remarkable in that the 8-atom and 16-atom clusters are very different but give almost identical results. In fact, half of the valence electrons are in the  $L$  representations of the 16-atom cluster, representations that are wholly absent in the 8-atom cluster. The 8-atom cluster has 8 electrons in the  $\Gamma$  representations and 24 electrons in the  $X$  representations, while the 16-atom cluster also has 32 electrons in the  $L$  representations. These numbers are exactly proportional to the weights of the special points, determined according to the Chadi and Cohen recipe for  $\Gamma$ ,  $X$ , and  $L$  (Table I).

TABLE IV. Nonrelativistic eigenvalues (eV) for silicon periodic clusters with different sizes. The cluster labeled as *MT/cell* has constant potential in the region between the cell boundary and the inscribed sphere. The values of the constant are different for the Si and empty cells. In the other clusters, the potential in that region is variational in three parameters. The full band eigenvalues are those of Hybertsen and Louie (see Ref. 38) and the experimental eigenvalues are quoted by them.

	Present calculations				Full band	Expt.
	2-atoms	8-atom <i>MT/cell</i>	8-atom	16-atom		
$\Gamma_{1,v}$	-11.74	-12.10	-11.86	-11.88	-11.92	-12.5±0.6
$L'_{2,v}$				-9.56	-9.58	-9.3±0.4
$X_{1,v}$		-7.94	-7.76	-7.79	-7.77	
$L_{1,v}$				-7.00	-6.97	-6.7±0.2
$X_{4,v}$		-2.99	-2.80	-2.80	-2.86	-2.9
$L'_{3,v}$				-1.14	-1.21	-1.2±0.2
$\Gamma_{25,v}$	0.47	0.00	0.00	0.00	0.00	0.0
$X_{1,c}$		0.29	0.48	0.46	0.71	1.30
$L_{1,c}$				1.15	1.55	2.1
$\Gamma_{15,c}$	2.35	2.01	2.26	2.25	2.57	3.37
$\Gamma_{2,c}$	3.29	2.88	3.00	2.84	3.29	4.2
$L_{3,c}$				3.26	3.40	3.9±0.1
$L'_{2,c}$				6.86		
$\Gamma_{1,c}$	6.31	7.32	7.27	7.28		

Compared to experiment, our eigenvalues for Si and Ge are very good, for the valence states, and shifted downwards, for the conduction states. The downwards shift of the calculated conduction band is very well known and an unavoidable feature of the *local-density approximation*<sup>38</sup> for all semiconductors. Paying careful attention at the entries of those tables, one observes that the conduction bands are not only shifted but deformed as well. Therefore, in comparing calculated results with experiment we will be mainly interested in the valence states, where a LDA calculation is meaningful.

### B. Perfect diamond

The calculated eigenvalues for diamond are in Table VI, compared with a full band calculation of Schmid and

TABLE V. Nonrelativistic eigenvalues (eV) for germanium periodic clusters with different sizes. The full band eigenvalues are those of Hybertsen and Louie (see Ref. 38) and the experimental eigenvalues are quoted by them.

	Present calculations			Full band	Expt.
	2-atom	8-atom	16-atom		
$\Gamma_{1,v}$	-12.32	-12.49	-12.48	-12.50	-12.6
$L'_{2,v}$			-10.32	-10.38	-10.6±0.5
$X_{1,v}$		-8.58	-8.56	-8.57	
$L_{1,v}$			-7.50	-7.40	-7.7±0.2
$X_{4,v}$		-3.11	-3.11	-3.03	-3.15±0.2
$L'_{3,v}$			-1.39	-1.38	-1.4±0.3
$\Gamma_{25,v}$	0.42	0.00	0.00	0.00	0.0
$L_{1,c}$			0.27	0.52	0.74
$X_{1,c}$		0.53	0.49	0.80	1.3±0.2
$\Gamma_{2,c}$	1.00	0.61	0.61	0.74	0.89
$\Gamma_{15,c}$	2.33	2.27	2.27	2.58	3.21
$L_{3,c}$			3.58	3.74	4.3±0.2
$\Gamma_{1,c}$	4.84	5.89	5.78		

Christensen.<sup>39</sup> Again, we observe that the calculated results converge fast with the cluster size. In Table VII we also compare our calculated results with experiment. The bottom of the valence band ( $\Gamma_{1,v}$ ) was formerly set at -24.2 eV,<sup>40</sup> but nowadays the number -21 eV is preferred,<sup>41</sup> in close agreement with our result. Our eigenvalue for  $L_{2,v}$  also agrees with experiment. The energy level at -12.8 eV that was interpreted as  $L_{1,v}$  is much closer to our  $X_{1,v}$ . For the conduction states our calculated results again suffer from the LDA deficiencies.

### C. Diamond, Si, and Ge with native interstitial and vacancy

For diamond, Si, and Ge we calculated the energy levels for clusters with vacancies and native interstitials. Because of the defect, the symmetry group is now reduced

TABLE VI. Nonrelativistic eigenvalues (eV) for diamond periodic clusters with different sizes.

	Present calculations			Full band <sup>a</sup>
	2-atom	8-atom	16-atom	
$\Gamma_{1,v}$	-21.96	-21.28	-21.28	-21.39
$L'_{2,v}$			-15.44	-15.56
$L_{1,v}$			-13.43	-13.47
$X_{1,v}$		-12.61	-12.61	-12.69
$X_{4,v}$		-6.25	-6.24	-6.34
$L'_{3,v}$			-2.73	-2.77
$\Gamma_{25,v}$	0.53	0.00	0.00	0.00
$X_{1,c}$		4.38	4.38	4.78
$\Gamma_{15,c}$	4.97	4.96	4.97	5.66
$L_{3,c}$			8.25	8.35
$L_{1,c}$			8.57	9.03
$\Gamma'_{2,c}$	12.93	12.79	12.79	13.50

<sup>a</sup>Reference 39.

TABLE VII. Calculated results for diamond, Si, and Ge compared with experiment (in eV). The top of the valence band is the energy reference. The experimental values are those of Ref. 41.

		Calculated	Expt.
Diamond	$\Gamma_{1,v}$	-21.28	-21±1
	$L_{2,v}$	-15.44	-15.2±0.3
	$L_{1,v}(X_{1,v})$	-13.43(-12.61)	-12.8±0.3
	$\Gamma_{15,c}$	4.97	6.0±0.2
	$\Gamma_{2,c}$	12.79	15.3±0.5
Diamond:Vacancy	Peak II	-13.5	
	Peak I	-4.4	
Diamond:C interstitial	Peak III	-24.0	-24.2 <sup>a</sup>
	hyperdeep	-22.33	
	Peak II	-14.0	
	Peak I	-2.8	
Si		See Table IV	
Si:Vacancy	Peak II	-7.7	
	Peak I	-1.8	
Si:Si interstitial	Peak III	-13.2	
	hyperdeep	-12.58	
	Peak II	-8.3	
	Peak I	-2.5	
Ge		See Table V	
Ge:Vacancy	Peak II	-8.5	
	Peak I	-2.1	
Ge:Ge interstitial	Peak III	-13.8	
	hyperdeep	-13.19	
	Peak II	-9.60	
	Peak I	-1.60	

<sup>a</sup>The bottom of the valence band cited by Ref. 40 is here interpreted as an interstitial level.

TABLE VIII. Nonrelativistic eigenvalues (eV) for ZnS and ZnSe periodic clusters with different sizes. The clusters labeled as *MT/cell* have constant potential in the region between the cell boundary and the inscribed sphere. Different cells have different constants.

	ZnS			ZnSe		
	8-atom <i>MT/cell</i>	16-atom <i>MT/cell</i>	Full band <sup>a</sup>	8-atom <i>MT/cell</i>	16-atom <i>MT/cell</i>	Full band <sup>b</sup>
$\Gamma_{1,v}$	-12.65	-12.65	-13.11	-12.59	-12.59	-12.86
$L_{1,v}$		-11.68	-12.16		-11.74	-12.06
$X_{1,v}$	-11.33	-11.33	-11.84	-11.44	-11.43	-11.79
<i>s</i> (average)	-11.66	-11.67	-12.16	-11.73	-11.73	-12.06
$\Gamma_{15,d}$	-7.01	-7.03	-6.55	-7.45	-7.49	-7.86
$X_{3,d}$	-6.99	-7.02		-7.41	-7.45	
$L_{3,d}$		-6.93			-7.35	
$X_{5,d}$	-6.72	-6.74		-7.23	-7.27	
$\Gamma_{12,d}$	-6.70	-6.72	-0.609	-7.24	-7.28	-7.50
$L_{3,d}$		-6.67			-7.28	
$X_{2,d}$	-6.60	-6.62		-7.13	-7.18	
$L_{1,d}$		-6.54			-7.10	
$X_{1,d}$	-6.44	-6.47		-6.99	-7.03	
Zn 3 <i>d</i> (average)	-6.74	-6.76	-6.37	-7.24	-7.28	-7.72
$L_{1,v}$		-5.12	-5.38		-5.23	-5.21
$X_{3,v}$	-4.50	-4.51	-4.70	-4.82	-4.84	-4.82
$X_{5,v}$	-2.00	-2.00	-2.25	-2.13	-2.13	-2.20
$L_{3,v}$		-0.66	-0.88		-0.76	-0.87
$\Gamma_{15,v}$	0.00	0.00	0.00	0.00	0.00	0.00
$\Gamma_{1,c}$	1.90	1.88	1.81	1.48	1.46	1.45
$L_{1,c}$		3.25	3.05		2.48	2.63
$X_{1,c}$	3.29	3.25	3.18	2.78	2.74	2.88
$X_{3,c}$	4.13	4.11	3.87	3.32	3.31	3.47
$\Gamma_{15,c}$	6.29	6.28	6.19	5.56	5.54	5.77
$L_{3,c}$		6.87	6.76		6.21	6.36

<sup>a</sup>Reference 48.

<sup>b</sup>Reference 49.

to  $T_d$ . The defect energy levels are represented by the top vertical lines in Figs. 1–3. In those figures, the energy levels of the perfect crystal are represented by the vertical lines in the bottom. In drawing the vertical lines representing the energy levels for the perfect and the defect clusters, one must face the problem of finding a common energy reference for the two calculations. We proceeded in the following way. The perfect cluster was also calculated with the reduced symmetry  $T_d$ . Under this reduction, the valence state  $L'_3$  becomes the superposition of  $e$ ,  $t_1$ , and  $t_2$ , according to Table III. The wave functions of  $e$  and  $t_1$  were almost zero at the site where the defect was to be placed. This means that, among the many defect cluster levels, these are the best representations of the pure crystal states. Accordingly, the energy levels of the defect were shifted so that  $e$  and  $t_1$  coincided with  $L'_3$  of the perfect cluster. It must be said that this is common procedure in defect calculations.<sup>42</sup>

Representing the density of states (DOS) corresponding to any level by a Gaussian, we plot in the figures the differential density of states, namely the DOS in the defect cluster minus the DOS of the perfect cluster. The energies for which the differential DOS is positive would be the energies to be observed experimentally as indicating the presence of the defect. We used very broad

Gaussians to construct Figs. 1–3, so as to enhance only the most important features.

Figures 1(a)–3(a) represent the case of the vacancies. There are two positive peaks in the valence band (negative energies), the highest peak being just barely observable in the cases of Si and Ge [Figs. 2(a) and 3(a)]. For the interstitials [Figs. 1(b)–3(b)], there are three positive peaks, the lowest of which is at an energy even lower than the bottom of the valence band. This lowest peak is due to the first  $a_1$  level (hyperdeep level),<sup>43</sup> which is lower than the bottom of the valence band ( $\Gamma_1$ ). The energies of the peaks and that of the hyperdeep level are in Table VII. In the case of diamond, the existence of the hyperdeep level and of the lowest peak are a natural explanation for the value  $-24.2$  eV formerly attributed to the diamond bandwidth.<sup>40</sup>

#### D. ZnS and ZnSe

The periodic-cluster energy levels of ZnS and ZnSe are in Table VIII. Contrary to the case of Si and Ge, a comparison of our levels with the results of recent full band calculations is not as good, and one observes shifts of as much as 0.5 eV for the lowest valence states. Different calculation techniques might be responsible for those differences. We observed<sup>18</sup> that the position of the

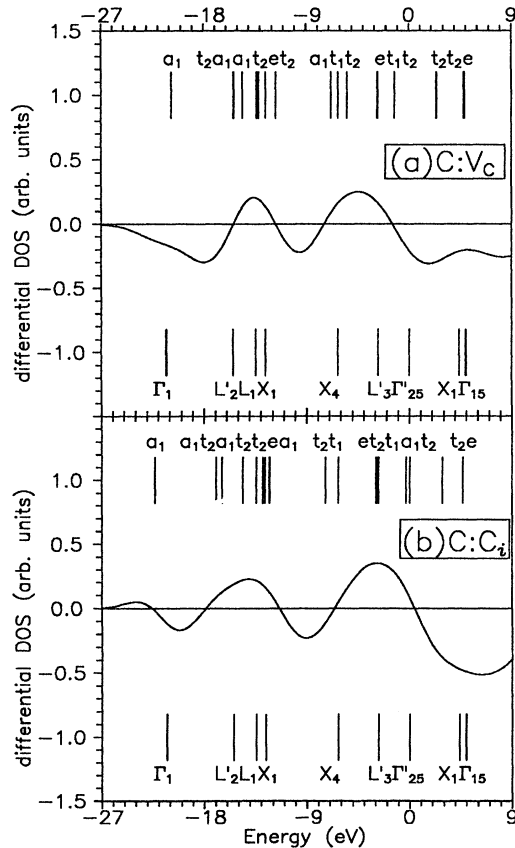


FIG. 1. Diamond. Density of states of the defect minus that of the perfect cluster. (a) Vacancy; (b) interstitial. The top vertical lines are the energy levels for the cluster with defect. The lines in the bottom are the energy levels for the perfect cluster.

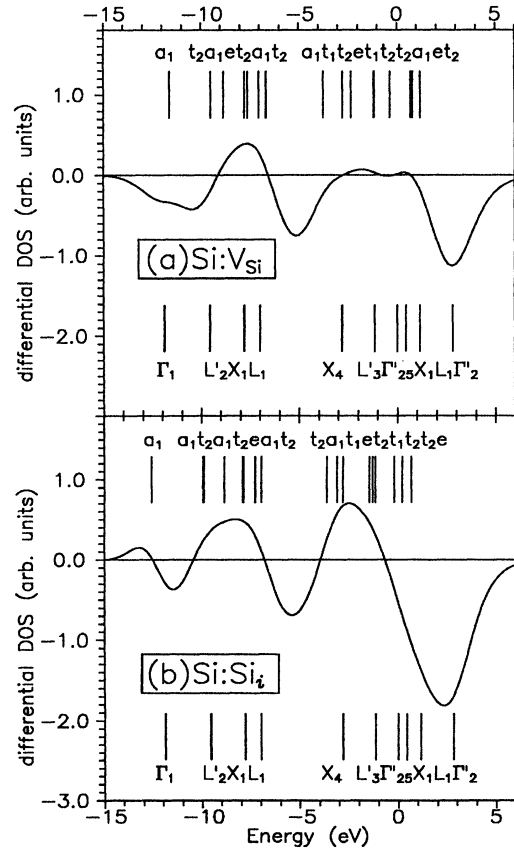


FIG. 2. Si. Density of states of the defect minus that of the perfect cluster. (a) Vacancy; (b) interstitial. The top vertical lines are the energy levels for the cluster with defect. The lines in the bottom are the energy levels for the perfect cluster.

valence bands depends much on the hybridization of the Zn  $3d$  wave functions with the anion  $s$  and  $p$  wave functions. If the mixture of these states is much too large, the anion will gain extra electronic charge, which raises its bands and lowers the Zn  $3d$  bands. The amount of hybridization is small (among the 10  $d$  electrons, about 0.6 move out of Zn) but its calculation depends much on how well the  $d$  wave functions are expanded.

To compare our calculated results with experiment, one cannot forget that, within the LDA, the excitation energy is the eigenvalue at half occupation, not the eigenvalue at full occupation of the level. The difference between the half and full occupation eigenvalues can be readily interpreted as the electrostatic self-interaction (plus an exchange-correlation contribution) of the hole that is formed in promoting the electron to the conduction band.<sup>18,19</sup> For a Bloch state hole, that is, a hole that spreads in the whole crystal, the self-interaction is zero, but for a hole much denser in just one atom, the self-interaction can be important.<sup>20</sup> To have an idea of how important the self-interaction can be, we present in Table IX the atomic self-interaction corrections for the transitions we are dealing with. These corrections are the difference between the excitation energy to the first unoccupied (or partially occupied) level, calculated at the

TABLE IX. Atomic self-interaction corrections (eV).

Se( $3d-4p$ ) = -5.17	Se( $4s-4p$ ) = -0.10
Ge( $4s-4p$ ) = -0.14	
Zn( $3d-4s$ ) = -2.30	
S( $3s-3p$ ) = -0.07	
Si( $3s-3p$ ) = -0.10	
C( $2s-2p$ ) = -0.02	

ground state and calculated with 0.5 promoted electrons. We observe in Table IX that the self-interaction becomes especially important for the  $d$  electrons, and that it increases with atomic number.

To calculate the self-interaction correction in the cluster levels, we had to make calculations reducing the symmetry to that of the point group  $T_d$  and promoting 0.5 electrons to the first conduction state. The self-interaction correction was set equal to the difference between the excitation energy in the cluster with reduced symmetry (and 0.5 electrons promoted) and that in the ground-state cluster. We obtained the following values for the self-interaction correction, all with respect to the

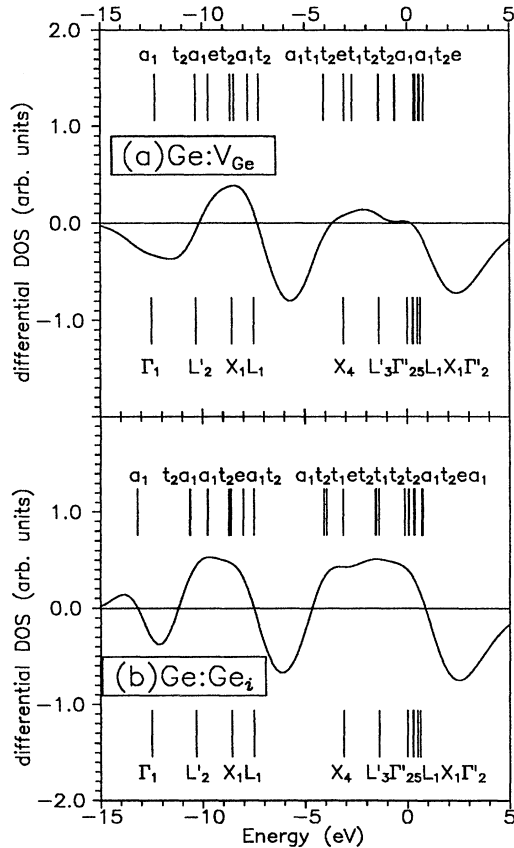


FIG. 3. Ge. Density of states of the defect minus that of the perfect cluster. (a) Vacancy; (b) interstitial. The top vertical lines are the energy levels for the cluster with defect. The lines in the bottom are the energy levels for the perfect cluster.

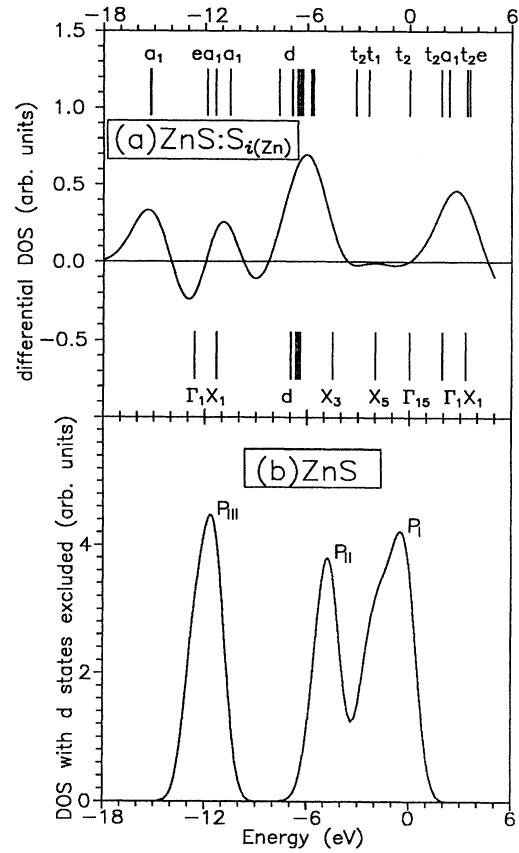


FIG. 4. ZnS. (a) Density of states of the  $S_{i(Zn)}$  interstitial minus that of the perfect cluster. The top vertical lines are the energy levels for the cluster with defect. The lines in the bottom are the energy levels for the perfect cluster. (b) Density of states for the perfect ZnS cluster with 16 atoms, excluding the Zn  $3d$  levels.

top of the valence band:  $Zn\ 3d(ZnS) = -2.20$  eV,  $Zn\ 3d(ZnSe) = -2.25$  eV,  $Se\ 3d(ZnSe) = -6.4$  eV,  $S\ 3s(ZnS) = -0.66$  eV,  $Se\ 4s(ZnSe) = -0.68$  eV, all other less than 0.1 eV. The case of the  $S\ 4s$  and  $Se\ 4s$  self-interaction corrections, corresponding to the bottom of the valence, is very interesting. In the cluster with eight atoms (four atoms S or Se), the valence band at the bottom is made of levels  $\Gamma_1$  and  $X_1$ . In reducing the symmetry,  $X_1$  becomes  $a_1 + e$  and it is this  $a_1$  level, and not  $a_1(\Gamma_1)$ , that is much denser in the S (or Se) at the origin. Therefore, in promoting 0.5 electrons from the  $s$  band to the conduction band, it is the  $a_1(X_1)$  level that moves downwards and defines the self-interaction.

Table X compares the results of the perfect clusters of ZnS and ZnSe with experiment. Aside from the huge peak due to the  $Zn\ 3d$  electrons, Ley *et al.*<sup>44</sup> were able to distinguish three other valence density-of-state peaks in their experiment: peak  $P_{III}$  is the lowest in energy and peak  $P_I$  the highest. In Figs. 4(b) and 5(b) we plot our calculated valence density of states, with  $Zn\ 3d$  levels excluded, now using Gaussians with widths similar to those that Ley *et al.* used to interpret their experiment (about 0.5 eV). Peak  $P_{III}$  is centered at the weighted average of the energies of the lowest valence states ( $\Gamma_{1,v}, L_{1,v}, X_{1,v}$  in

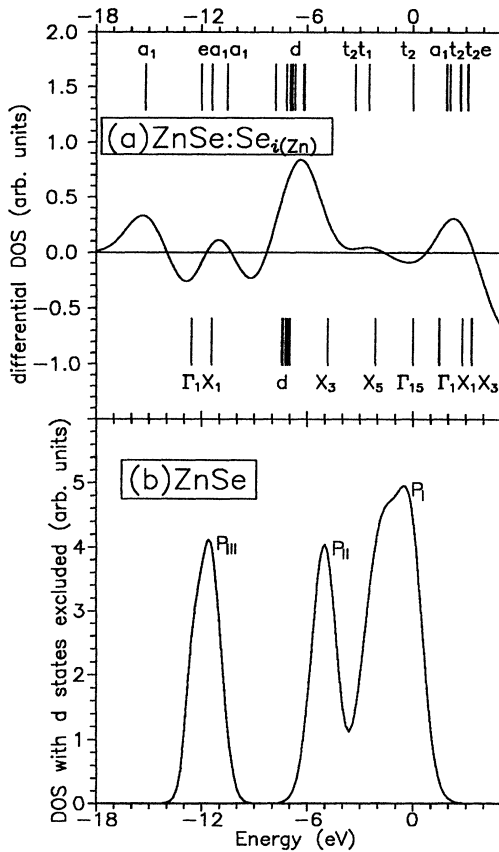


FIG. 5. ZnSe. (a) Density of states of the  $Se_{i(Zn)}$  interstitial minus that of the perfect cluster. The top vertical lines are the energy levels for the cluster with defect. The lines in the bottom are the energy levels for the perfect cluster. (b) Density of states for the perfect ZnSe cluster with 16 atoms, excluding the  $Zn\ 3d$  levels.

the cluster with 16 atoms). The energy at the peak plus the self-interaction correction is our entry in the column labeled "Calc." in Table X. In peak  $P_I$  Ley *et al.* were able to distinguish a structure and set energy values for the states  $X_{5,v}$  and  $L_{3,v}$ . In peak  $P_{II}$  the level structure was less clear so that we can only compare the peak energy with our calculated value in Figs. 4(b) and 5(b). The comparison of our calculated results with experiment in Table X follows the pattern of the preceding calculations

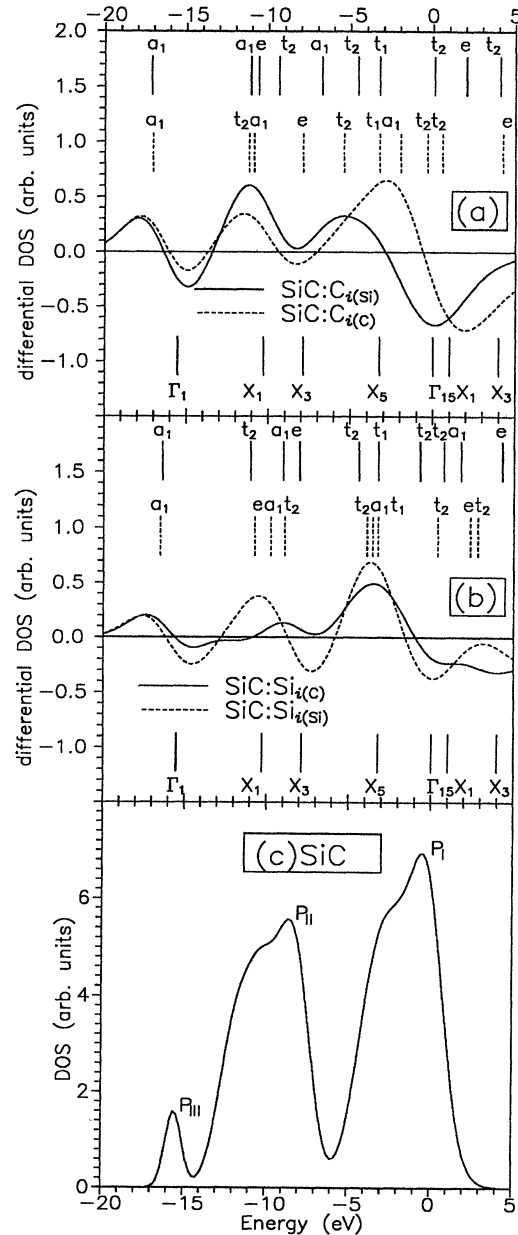


FIG. 6. SiC. (a) Density of states of the C interstitial minus that of the perfect cluster. Solid line:  $C_{i(Si)}$ . Dashed line:  $C_{i(C)}$ . The top vertical lines are the energy levels for the cluster with defect. The lines in the bottom are the energy levels for the perfect cluster. (b) Si interstitial. Solid line:  $Si_{i(C)}$ . Dashed line:  $Si_{i(Si)}$ . (c) Density of states for the perfect SiC cluster with 16 atoms.

TABLE X. Calculated results for ZnS and ZnSe compared with experiment (in eV). The top of the valence band is the energy reference. The calculated results marked with (\*) were corrected for the self-interaction (see text).

		Calc.	Expt.
ZnS	S 3s peak ( $P_{III}$ )	-12.32(*)	-12.4 <sup>a</sup>
	Zn 3d	-8.94(*)	-9.03±0.15 <sup>a</sup>
	S 3p lower peak ( $P_{II}$ )	-4.8	-4.9 <sup>a</sup>
	$X_{5,v}$	-2.00	-2.5±0.3 <sup>a</sup>
	$L_{3,v}$	-0.66	-1.4±0.4 <sup>a</sup>
	$\Gamma_{1,c}$ gap	1.88	3.80 <sup>b</sup>
ZnS:S interstitial	Peak III	-15.4	
	hyperdeep	-15.22	
	Peak II	-10.9	
	Peak I	-6.0	
ZnSe	Se 3d	-53.28(*)	-53.50±0.15 <sup>a</sup>
	Se 3s peak ( $P_{III}$ )	-12.41(*)	-12.5 <sup>c</sup>
	Zn 3d	-9.49(*)	-9.20±0.15 <sup>a</sup>
	Se 3p lower peak ( $P_{II}$ )	-5.0	-5.2 <sup>a</sup>
	$X_{5,v}$	-2.13	-2.1±0.3 <sup>a</sup>
	$L_{3,v}$	-0.76	-1.3±0.3 <sup>a</sup>
ZnSe:Se interstitial	$\Gamma_{1,c}$ gap	1.46	2.82 <sup>b</sup>
	Peak III	-15.4	-15.2±0.6 <sup>a,d</sup>
	hyperdeep	-15.21	
	Peak II	-11.0	
	Peak I	-6.4	

<sup>a</sup>See Ref. 44.

<sup>b</sup>See Ref. 50.

<sup>c</sup>See Ref. 51.

<sup>d</sup>The bottom of the valence band is here interpreted as an interstitial energy level.

for diamond, Si, and Ge: it is very good for the valence states but suffers from the LDA deficiency for the conduction states.

#### E. ZnS and ZnSe with native anion interstitial

The calculated differential densities of states for native anion interstitials in ZnS and ZnSe are plotted in Figs. 4(a) and 5(a), together with the energy levels for the perfect and defect clusters. These calculations were made with the clusters of eight atoms. In reducing the symmetry to that of the point group  $T_d$ , we observed that the top of the valence band  $t_2(\Gamma_{15})$  and the energy level just below  $t_1(X_5)$  had wave functions that stayed away from the defect. We could use either as a common energy reference for the perfect and defect clusters; we chose the top of the valence band.

Again, we observe three positive peaks in the differential DOS of the valence band, the lowest corresponding to a hyperdeep defect level. Contrary to the case of native interstitials in diamond, Si, and Ge [Figs. 1(a)–3(a)], the highest valence peak is now made of Zn 3d states neighboring the anion interstitial; therefore, much deeper into the valence bands. The results for the interstitials in ZnS and ZnSe are in Table X. As in the case of diamond, the experimental value of 15.2 eV formerly attributed to the valence bandwidth is reinterpreted as the hyperdeep interstitial level.

#### F. SiC: Perfect and interstitials

Table XI and Fig. 6 show our main results for SiC, pure and with C and Si interstitials in C and Si neighbor-

TABLE XI. Results for SiC (in eV). The top of the valence band is the energy reference.

	This work		Other calculation and expt.
Peak III ( $\Gamma_1$ )	-15.53		-15.36 <sup>a</sup>
$L_{1,v}$	-11.79		
$X_{1,v}$	-10.29		
$L_{1,v}$	-8.84		
Peak II	-8.6		-8.5 <sup>b</sup> , -8.4 <sup>c</sup>
$X_{3,v}$	-7.92		
$X_{5,v}$	-3.25		-3.8 <sup>c</sup>
$L_{3,v}$	-0.95		
$\Gamma_{15,v}$	0.0		
$X_{1,c}(\text{gap})$	0.97		2.42 <sup>d</sup>
$X_{3,c}$	3.93		
$L_{1,c}$	5.46		
$\Gamma_{1,c}$	6.30		
Si interstitial	:Si <sub>i(Si)</sub>	:Si <sub>i(C)</sub>	experimental
Peak III	-17.6	-17.4	-18.1 <sup>c</sup> , -(17.5–19.2 <sup>e</sup> )
hyperdeep( $a_1$ )	-16.52	-16.40	
Peak II	-10.5	-9.1	
Peak I	-3.7	-3.5	
C interstitial	:C <sub>i(C)</sub>	:C <sub>i(Si)</sub>	experimental
Peak III	-17.8	-17.9	-18.1 <sup>c</sup> , -(17.5–19.2 <sup>e</sup> )
hyperdeep ( $a_1$ )	-17.10	-17.11	
Peak II	-11.5	-11.2	
Peak I	-2.8	-5.4	

<sup>a</sup>Calculated—Ref. 47.

<sup>b</sup>Reference 45.

<sup>c</sup>Reference 46.

<sup>d</sup>Reference 52.

<sup>e</sup>Reference 53.

hoods. The density of states [Fig. 6(c)] was calculated by adding narrow Gaussians centered at the levels of the 16-atom cluster, while the defect differential density of states [Figs. 6(a) and 6(b)] was based in the 8-atom clusters.

The interpretation of x-ray data on SiC has been severely handicapped by the wrong assumption that the valence bandwidth is, as measured, on the order of 18 eV.<sup>45,46</sup> Modern band-structure calculations set the lowest valence level ( $\Gamma_{1,v}$ ) at  $-15.36$  eV (Ref. 47) or  $-15.53$  eV, as we calculated. The measured bandwidth of about 18 eV is probably due to C or Si interstitials, both able to produce hyperdeep levels, as explained in Figs. 6(a) and 6(b), and in Table XI. The x-ray peak at  $-8.4$  eV is clearly equivalent to our peak II of the DOS curve. Another clear structure in the x-ray spectrum, the peak at  $-3.8$  eV, which was interpreted as the  $X_{5,v}$  level,<sup>46</sup> compared well with our calculated value.

As in the case of the other semiconductors, the calculated band gap is clearly in error. Though the LDA calculation of the gap is consistently in error, it is able at

least to correctly distinguish between a direct and indirect gap.

## V. CONCLUSIONS

Our study of diamond, Si, Ge, ZnS, ZnSe, SiC pure and with native defects, by means of the cellular method combined with the periodic-cluster technique, confirms the usefulness and precision of this methodology. Our results for the valence states seem to be excellent, once more showing that the local-density approximation is a useful tool for interpreting experiment. For the conduction states, our results repeat the common failure of the LDA: unduly small gaps and band deformation.

For all the studied compounds, we could find a hyperdeep interstitial level.<sup>43</sup> In the cases of diamond, ZnSe, and SiC, this level may be the reason for a wrong value experimentally assigned to the valence bandwidth.

In the case of the Zn compounds, and just in that case, the self-interaction correction is very important in placing the Zn  $3d$  bands at their correct positions.

\*Permanent address: Departamento de Física, Universidade Federal de Minas Gerais, Caixa Postal 702, 30161 Belo Horizonte, Brazil.

<sup>1</sup>A. M. Dobrotvorskii and R. A. Evarestov, Phys. Status Solidi B **66**, 83 (1974).

<sup>2</sup>A. Zunger, J. Phys. C **7**, 96 (1974).

<sup>3</sup>A. H. Harker and F. P. Larkins, J. Phys. C **12**, 2487 (1979); **12**, 2497 (1979).

<sup>4</sup>J. K. Freericks and L. M. Falicov, Phys. Rev. B **42**, 4960 (1990).

<sup>5</sup>A. B. Harris and R. V. Lange, Phys. Rev. **157**, 295 (1967).

<sup>6</sup>U. Lindefelt and A. Zunger, Phys. Rev. B **26**, 846 (1982).

<sup>7</sup>G. A. Baraff and M. Schluter, Phys. Rev. B **19**, 4965 (1979).

<sup>8</sup>W. V. M. Machado, D. L. Kinoshita, and L. G. Ferreira, Phys. Rev. B **41**, 10 735 (1990).

<sup>9</sup>N. Gemma, J. Phys. C **17**, 2333 (1984).

<sup>10</sup>K. H. Johnson and F. C. Smith, Jr., Phys. Rev. B **5**, 831 (1972).

<sup>11</sup>A. Baldereschi, Phys. Rev. B **7**, 5212 (1973).

<sup>12</sup>D. J. Chadi and M. L. Cohen, Phys. Rev. B **8**, 5747 (1973).

<sup>13</sup>H.J. Monkhorst and J. D. Pack, Phys. Rev. B **13**, 5188 (1976).

<sup>14</sup>S. Froyen, Phys. Rev. B **39**, 3168 (1989).

<sup>15</sup>J. Moreno and J. M. Soler, Phys. Rev. B **45**, 13 891 (1992).

<sup>16</sup>J. M. Luttinger and W. Kohn, Phys. Rev. **97**, 869 (1955).

<sup>17</sup>R. P. Messmer and G. D. Watkins, Phys. Rev. Lett. **25**, 656 (1970); Phys. Rev. B **7**, 2568 (1973); S. G. Louie, M. Schluter, J. R. Chelikowski, and M. L. Cohen, *ibid.* **13**, 1654 (1976); U. Lindefelt, J. Phys. C **11**, 85 (1978); Y. M. Gu, L. Fritsche, and N. E. Christensen, Phys. Status Solidi B **159**, 617 (1990); O. Sugino and A. Oshiyama, Phys. Rev. Lett. **68**, 1858 (1992).

<sup>18</sup>L. G. Ferreira and M. L. De Siqueira, Phys. Rev. B **34**, 5315 (1986).

<sup>19</sup>J. A. Kintop, W. V. M. Machado, and L. G. Ferreira, Phys. Rev. A **43**, 3348 (1991).

<sup>20</sup>A. Zunger, Phys. Rev. Lett. **50**, 1215 (1983).

<sup>21</sup>G. F. Koster, in *Solid State Physics: Advances in Research and Applications*, edited by H. Ehrenreich, F. Seitz, and D. Turn-

bull (Academic, New York, 1958), Vol. 5, p. 174.

<sup>22</sup>J. C. Slater, *Quantum Theory of Molecules and Solids* (McGraw-Hill, New York, 1959), Vol. 2, p. 347.

<sup>23</sup>L. G. Ferreira, J. A. Kintop, and W. V. M. Machado, J. Phys. B **21**, 4063 (1988).

<sup>24</sup>J. C. Slater, Phys. Rev. **45**, 794 (1934).

<sup>25</sup>S. L. Altmann, Proc. R. Soc. London Ser. A **244**, 141 (1958).

<sup>26</sup>X.-G. Zhang and W. H. Butler, Phys. Rev. Lett. **68**, 3753 (1992); S. Antoci, J. Chem. Phys. **63**, 697 (1975). There are other versions of the cellular method. Even in the small Brazilian scientific community there are versions of the cellular method with different space partitioning and wave-function expansions.

<sup>27</sup>For instance, in optics: M. A. A. Pudensi and L. G. Ferreira, J. Opt. Soc. Am. **72**, 126 (1982).

<sup>28</sup>R. S. Leigh, Proc. Phys. Soc. London Sect. A **69**, 388 (1956).

<sup>29</sup>H. Schlosser and P. M. Marcus, Phys. Rev. **131**, 2529 (1963).

<sup>30</sup>O. Gunnarsson and B. I. Lundqvist, Phys. Rev. B **13**, 4274 (1976).

<sup>31</sup>J. P. Perdew and A. Zunger, Phys. Rev. B **23**, 5048 (1981).

<sup>32</sup>L. G. Ferreira, A. Fazzio, H. Closs, and L. M. Bressanin, Int. J. Quantum Chem. **16**, 1021 (1979).

<sup>33</sup>M. A. P. Lima and L. G. Ferreira, Phys. Rev. A **22**, 343 (1980).

<sup>34</sup>H. Wendel and R. M. Martin, Phys. Rev. B **19**, 5251 (1979).

<sup>35</sup>J. Harris, Phys. Rev. B **31**, 1770 (1985).

<sup>36</sup>N. Chetty, K. Stokbro, K. W. Jacobsen, and J. K. Norskov, Phys. Rev. B **46**, 3798 (1992).

<sup>37</sup>J. F. Janak, Phys. Rev. B **18**, 7165 (1978).

<sup>38</sup>M. S. Hybertsen and S. G. Louie, Phys. Rev. Lett. **55**, 1418 (1985); Phys. Rev. B **30**, 5777 (1984).

<sup>39</sup>U. Schmid and N. E. Christensen, quoted by R. Hott, Phys. Rev. B **44**, 1057 (1991).

<sup>40</sup>F. R. McFeely, S. P. Kowalczyk, L. Ley, R. G. Cavell, R. A. Pollak, and D. A. Shirley, Phys. Rev. B **9**, 5268 (1974).

<sup>41</sup>F. J. Himpsel, J. F. van der Veen, and D. E. Eastman, Phys. Rev. B **22**, 1967 (1980).

- <sup>42</sup>A. Fazio and J. R. Leite, *Phys. Rev. B* **21**, 4710 (1980).
- <sup>43</sup>G. A. Baraff, M. Schluter, and G. Allan, *Phys. Rev. B* **27**, 1010 (1983); M. Lannoo and M. Schluter, *ibid.* **31**, 5468 (1985); S. Goettig and C. G. Morgan-Pond, *ibid.* **42**, 11 730 (1990); **42**, 11 743 (1990).
- <sup>44</sup>L. Ley, R. A. Pollak, F. R. McFeely, S. P. Kowalczyk, and D. A. Shirley, *Phys. Rev. B* **9**, 600 (1974).
- <sup>45</sup>I. I. Zhukova, V. A. Fomichev, A. S. Vinogradov, and T. M. Zinkina, *Fiz. Tverd. Tela* **10**, 1383 (1968) [*Sov. Phys. Solid State* **10**, 1097 (1968)].
- <sup>46</sup>V. V. Nemoshkalenko, V. G. Aleshin, M. T. Panchenko, and A. I. Senkevich, *Dokl. Akad. Nauk* **214**, 543 (1973) [*Sov. Phys. Dokl.* **19**, 38 (1974)].
- <sup>47</sup>K. J. Chang and M. L. Cohen, *Phys. Rev. B* **35**, 8196 (1987).
- <sup>48</sup>J. L. Martins, N. Trouillier, and S.-H. Wei, *Phys. Rev. B* **43**, 2213 (1991).
- <sup>49</sup>J. E. Bernard and A. Zunger, *Phys. Rev. B* **36**, 3199 (1987).
- <sup>50</sup>D. Theis, *Phys. Status Solidi B* **79**, 125 (1977).
- <sup>51</sup>J. R. Chelikowski, T. J. Wagener, J. H. Weaver, and A. Jin, *Phys. Rev. B* **40**, 9644 (1989).
- <sup>52</sup>*Landolt-Bornstein Tables*, edited by O. Madelung, M. Schulz, and H. Weiss (Springer, Berlin, 1982), Vol. 17a.
- <sup>53</sup>G. Wiech, in *Soft X-Ray Band Spectra and the Electronic Structures of Metals and Materials*, edited by D. J. Fabian (Academic, New York, 1968).